

1 Particle tracking in kaon electroproduction with
 2 cathode-charge sampling in multi-wire proportional
 3 chambers

4 P. Achenbach^{a,*}, C. Ayerbe Gayoso^a, J. C. Bernauer^a, R. Böhm^a, D. Bosnar^b,
 5 M. Bösza^a, L. Debenjak^c, M. O. Distler^a, A. Esser^a, I. Friščić^b, M. Gómez
 6 Rodríguez de la Paz^a, M. Makek^b, H. Merkel^a, U. Müller^a, L. Nungesser^a,
 7 J. Pochodzalla^a, M. Potokar^c, S. Sánchez Majos^a, B. S. Schlimme^a, S. Širca^c,
 8 M. Weinriefer^a

9 ^a*Institut für Kernphysik, Johannes Gutenberg-Universität Mainz, Germany*

10 ^b*Department of Physics, University of Zagreb, Croatia*

11 ^c*University of Ljubljana and Jožef Stefan Institute, Ljubljana, Slovenia*

12 **Abstract**

Wire chambers are routinely operated as tracking detectors in magnetic spectrometers at high-intensity continuous electron beams. Especially in experiments studying reactions with small cross-sections the reaction yield is limited by the background rate in the chambers. One way to determine the track of a charged particle through a multi-wire proportional chamber (MWPC) is the measurement of the charge distribution induced on its cathodes. In practical applications of this read-out method, the algorithm to relate the measured charge distribution to the avalanche position is an important factor for the achievable position resolution and for the track reconstruction efficiency. An algorithm was developed for operating two large-sized MWPCs in a strong background environment with multiple-particle tracks. Resulting efficiencies were determined as a function of the electron beam current and on the signal amplitudes. Because of the different energy-losses of pions, kaons, and protons in the momentum range of the spectrometer the efficiencies depend also on the particle species.

13 *Keywords:* Tracking and position-sensitive detectors, multi-wire proportional
 14 chambers, magnetic spectrometers, electron-induced coincidence experiments

15 *PACS:* 29.30.-h, 29.40.Gx

*Corresponding author. Tel.: +49-6131-3925831; fax: +49-6131-3922964.
 Preprint submitted to *Nucl. Instr. and Meth. in Phys. Res. A*

16 1. Introduction

17 Since long, high-resolution magnetic spectrometers for charged particles have
18 been used in nuclear and particle physics. Combined with suitable coordinate
19 detectors for tracking, such instruments can achieve the most accurate measure-
20 ment of kinematic quantities [1]. For focusing spectrometers the measurements
21 can be done in an detection area out of the line-of-sight to the target that is
22 shielded to some extent from background particles. At the two currently operat-
23 ing high-energy, high-intensity continuous electron beam accelerators MAMI in
24 Mainz, Germany, and CEBAF at Jefferson Lab (JLab), Virginia, wire chambers
25 are routinely operated as tracking detectors in magnetic spectrometers [2-4].

26 During the last decade, a class of strangeness production experiments rep-
27 resented by the $(e, e'K^+)$ reaction were realized at the spectrometer facilities of
28 both laboratories. The small cross-sections encountered in these reactions re-
29 quire high luminosities and in case of hypernuclear reactions the use of nuclear
30 targets up to the medium-mass region ($A \leq 52$). To maximise hypernuclear
31 yields, the spectrometers are operated at minimum forward angles, where back-
32 ground rates increase by several orders of magnitude, severely interfering with
33 the operation of the wire chambers.

34 In the pilot $(e, e'K^+)$ hypernuclear experiment at JLab, E89-009, a very high
35 rate of electrons associated with bremsstrahlung dominated the background in
36 the electron spectrometer and a very high rate of positrons from Dalitz pairs
37 dominated the particle flux in the kaon spectrometer, so that beam currents were
38 limited to below $1 \mu\text{A}$, giving an experimental luminosity, \mathcal{L} , of approximately
39 $0.001 \times 10^{36} \text{ cm}^2\text{s}^{-1}$ [5]. Even after a decade of optimizations the wire chambers
40 of the third generation experiment at JLab, E05-115 (HKS-HES), experienced
41 multiple tracks for a medium-mass target of 150 mg/cm^2 and beam currents of
42 several μA ($\mathcal{L} = 0.09 \times 10^{36} \text{ cm}^2\text{s}^{-1}$) that could not be resolved by the standard
43 tracking analysis with a track reconstruction efficiency higher than $\sim 50\%$ [6].

44 The operation of multi-wire proportional chambers (MWPCs) in the KAOS
45 spectrometer at MAMI is discussed in Section 2. It is described how the centre-

46 of-charge analysis method, well-established in single-track events, had to be
47 adapted to the multiple-track events. The strong variation in the charge distri-
48 butions and the ambiguity introduced by a large number of charge clusters per
49 event has lead to the development of a cluster and track-finding algorithm for
50 the MWPCs, which is presented in Sections 3 and 4. This algorithm succeeded
51 in resolving the multiple-track ambiguities with high efficiency. It was in-beam
52 tested with a set of dedicated efficiency counters which allowed to check the
53 validity of possible tracks. Results of the efficiency measurements are presented
54 in Section 5 and the application of the method is discussed in Section 6.

55 **2. Operation of the MWPCs**

56 Crucial requirements for the wire chamber operation in kaon electroproduc-
57 tion measurements are (i) high efficiency for minimum ionizing particles and
58 (ii) tracking capability for luminosities above $5 \times 10^{36} \text{ cm}^2 \text{ s}^{-1}$. The limit for
59 the second requirements depend strongly on the wire chamber geometry. It
60 is known that slow-moving ions from the avalanches around the anodes form
61 space charges that reduce the field. The effective voltage drop for a given par-
62 ticle rate increases with the anode pitch, with the distance between anode and
63 cathode plane, and with the gas gain [7]. Modern developments aim for MWPC
64 that resolve track coordinates with a spatial resolution of about $100 \mu\text{m}$ in a
65 very high-rate background up to a few MHz/cm^2 . Such chambers have small
66 chamber dimensions and are operated with low gas gain.

67 At the Institut für Kernphysik in Mainz, Germany, two large-sized MW-
68 PCs are operated by the A1 Collaboration as tracking detectors in the KAOS
69 spectrometer's hadron arm [8]. They were used before in several beam-times
70 at GSI for trajectory reconstruction at relativistic heavy ion experiments, de-
71 tecting successfully trajectories of pions and kaons as well as protons and heavy
72 nuclear fragments [9, 10]. Contrary to conventional MWPCs the multiplication
73 process in these chambers is divided into two steps, following a concept first
74 described by Breskin and co-workers [11]. During the electron scattering ex-

75 periments at MAMI the distribution of charge states of the ionizing particles
 76 as well as particle fluxes differ greatly from the situation at GSI. Typically the
 77 detector packages of spectrometers at electron machines are heavily shielded.
 78 At MAMI, the the shielding houses of the three-spectrometer facility consist
 79 of 40 cm thick boron carbide loaded concrete walls covered with a 5 cm thick
 80 lead layer on the inside. They weigh about 110 tons each [3]. For the shield-
 81 ing of the KAOS spectrometer polyethylene shields with 15% diboron trioxide
 82 by weight were used in combined system of shielding walls and ceiling covering
 83 20 m². The walls comprise a 10 cm thick neutron shield and a 5 cm thick lead
 84 layer. At the KAOS spectrometer the chambers, placed behind the analysing
 85 dipole magnet, are shielded by polyethylene walls and ceiling with 15% diboron
 86 trioxide by weight covering 20 m². The walls comprise a 10 cm thick neutron
 87 shield and a 5 cm thick lead layer. However, when a continuous-wave electron
 88 beam of several μA current is delivered to solid-state or cryogenic liquid targets
 89 situated in front of the dipole the chambers experience multiple tracks in almost
 90 every event due to high electromagnetic background radiation levels.

91 The two MWPCs, labelled M and L, have an active area of $1\,190 \times 340\text{ mm}^2$
 92 each. The chambers are schematically depicted in Fig. 1. They consist of a plane
 93 of anodes ($\varnothing = 20\ \mu\text{m}$ gold-plated tungsten wires, 2 mm spacing), symmetrically
 94 sandwiched between two orthogonal planes of cathodes in x - and y - direction
 95 ($\varnothing = 50\ \mu\text{m}$ gold-plated tungsten wires, 1 mm spacing) along with two meshes
 96 of woven fabrics of plastic coated with a nickel layer, making up two planar
 97 electrode structures, the grid (G) and the transfer (T) plane and two gaps,
 98 the pre-amplification gap and the transfer-gap. The wires of the anode plane
 99 are running in diagonal direction, making an angle of 45° with either cathode
 100 direction. Typical potentials applied to these electrodes are: $U_G = -9.1\text{ kV}$,
 101 $U_T = -2.0\text{ kV}$, $U_A = +4.0\text{ kV}$, with the cathodes grounded.

102 Despite modern alternatives like micro-pattern gas detectors, the use of
 103 multi-wire proportional chambers (MWPCs) is still an economical way to cover
 104 a large area with tracking devices for charged particles. MWPCs are especially
 105 attractive when the particle track can be recorded from a single chamber in

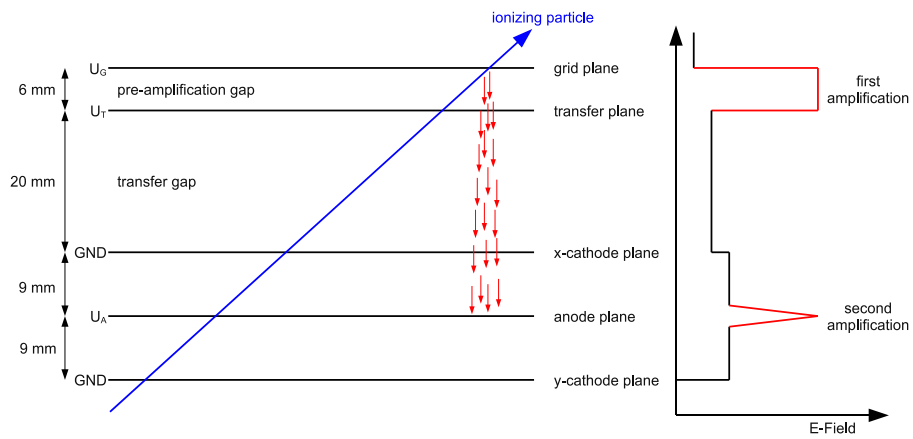


Figure 1: Schematic layout of the MWPCs with two-stage gas amplification. Each chamber consists of a plane of anodes ($\phi = 20 \mu\text{m}$ gold-plated tungsten wires, 2 mm spacing), symmetrically sandwiched between two orthogonal planes of cathodes ($\phi = 50 \mu\text{m}$ gold-plated tungsten wires, 1 mm spacing) along with two conducting grids, providing two gaps in front of the wire planes. On the right side a typical distribution of the electric field is shown. Electrons liberated in the pre-amplification gap are amplified before drifting through the transfer-gap, the transferred charge is amplified a second time at the anodes.

106 two orthogonal dimensions and when the required resolution is not significantly
107 finer than FWHM $\lesssim 1$ mm.

108 To determine the particle track the measured charge distributions induced
109 on the cathode wire planes of the MWPCs are analysed. Of the several known
110 methods for the bi-dimensional read-out of MWPCs, the induced-charge sam-
111 pling is well established since the 1970s [12]. However, even in single-track
112 operation, the choice of analysis method for the induced charge distributions on
113 the cathode strips or wires has consequences on the position resolution and the
114 track reconstruction efficiency [13]. The method can give good spatial resolu-
115 tion, but is compromised for multiple particles in one event as the signals can
116 get partially integrated, the wide charge distributions can overlap, and peaks
117 can get distorted.

118 Five cathode wires are connected together to one channel and are brought
119 to one charge-sensitive preamplifier making a total of 240 analogue channels in
120 x - and 70 analogue channels in y -direction. The preamplifiers provide a bipolar
121 output with a negative amplitude of up to 2.5 V. The pulse width is $\sim 2 \mu\text{s}$.
122 The signals are digitized by an ADC card addressed by a freely programmable
123 transputer module, mounted directly on the chamber. The ADC converts the
124 signal within $1.34 \mu\text{s}$ into 8 bit. Sixteen of the ADC channels are read out and
125 processed by one transputer. The transputer network system is connected to
126 a multi-link card inside a front-end computer. As the FWHM of an induced
127 cathode signal is known to be nearly equal to twice the anode-to-cathode gap,
128 this is 2×9 mm, clusters of signals in 3–5 channels are observed.

129 Particles from the target cross the MWPC planes with an angle of about (50
130 ± 20) $^\circ$ to the normal. The peak position of charges transferred from the pre-
131 amplification gap to the anodes is assumed to coincide with the impact point
132 of the trajectory of the ionizing particle with the grid plane. This position does
133 not depend on the angle of incidence of the particle's trajectory, whereas the
134 shape of the charge distribution is influenced.

135 The chambers are filled with a gas mixture of {84% Ar, 9% CO₂, 7%
136 C₄H₁₀} in volume concentration. Calibrated flow controllers are used to control

137 the amounts of the three gas components.

138 Details of the induced charge distributions depend on experimental param-
139 eters like track angles, particle species and velocities, and multiplicities, but
140 also on working conditions like gas mixture, high voltages, and the integration
141 gate width and timing. Therefore it is of practical importance to apply an algo-
142 rithm which gives the best position resolution and highest track reconstruction
143 efficiency. However, the choice of the analysis method depends heavily on the
144 experimental requirements.

145 **3. Cluster Analysis**

146 Fluctuations in the primary ionisation and electron diffusion along the drift
147 path lead to non-Gaussian charge distributions induced on the cathodes. The
148 distributions are further deteriorated by noisy channels, by multiple tracks in
149 the chamber, and by induced signals in the electronic chain. To relate the in-
150 duced charge distributions to the avalanche position, (i) the geometrical param-
151 eters of the chamber, (ii) the signal-to-noise ratio, and (iii) physical processes
152 of the ionization and avalanche formation had to be taken into account. Charge
153 distributions in both MWPCs taken with $2\mu\text{A}$ beam current on a 5 cm liq-
154 uid hydrogen target, corresponding to luminosities of $2.500 \times 10^{36} \text{ cm}^2\text{s}^{-1}$, are
155 shown in Figs. 2 and 3. Peak positions as indicated by vertical and horizontal
156 lines in the display were determined by the cluster algorithm discussed in this
157 Section.

158 The raw data are 8-bit ADC values, Q_i , for each read-out channel, x_i ,
159 in the x - and y -plane. As preamplifiers and ADCs vary along the planes,
160 each combination is assigned a gain factor c_i and a pedestal value p_i . In
161 few cases, where individual channels showed misbehaviour, caused *e.g.* by wire
162 ageing, their amplitudes were interpolated from both neighbouring channels.
163 Then “clusters” are defined by a group of neighbouring channels with detected
164 charges. A cluster has to consist of at least 2 channels and could include a
165 single channel below pedestal. At first each cluster is characterized by its de-

166 tected charge, $Q = \sum_n Q_i \cdot c_i$, its channel multiplicity, n , its centre-of-charge,
 167 $\bar{x} = (\sum_n Q_i \cdot c_i \cdot x_i) / (\sum_n Q_i \cdot c_i)$, its width, $\sigma = \sqrt{\sum_n |X_i - \bar{x}|^2 Q_i / Q}$, and its
 168 largest amplitude, Q_{max} , at channel x_{max} .

169 Because of the two amplification regions, as shown in Fig. 1 (right), and the
 170 large crossing angles of the particles, the liberated charges that are drifting from
 171 the pre-amplification plane will be displaced in the anode plane with respect to
 172 the weaker direct signal. The two separated charge localisations differ by a
 173 distance $x = d \tan \theta$, d being 35 mm. For a typical angle of $\theta = 55^\circ$ this distance
 174 was $x \cong 50$ mm corresponding to 10 channels. As the amplification of the direct
 175 signal was only partial, and the signal was induced on the cathodes at a much
 176 earlier time and thus got integrated only partially, a second peak in the charge
 177 distribution was not often observed, however, an asymmetry in the shape of the
 178 peak was regularly present in the signals. Because the drift time was regulated
 179 by the gas mixture and the high voltages, and the integration gate could get
 180 matched to this drift time, it was possible to minimize the appearance of double
 181 peaks and to reduce variation in cluster shapes. In Fig. 2 the peaks in the
 182 x -plane of MWPC M show features related to the two-stage amplification.

183 During the experiments sometimes charge distributions were observed, where
 184 satellite peaks were accompanying the physical peak, that was produced by a
 185 heavily-ionising light particle. Fig. 3 shows a charge distribution in the x -
 186 plane of MWPC M with satellite charges on both sides of a needle-like peak.
 187 The source of these peaks can be understood by the anode plane construction
 188 mounted in between the cathode planes and was identified as a capacitive cou-
 189 pling between anode and cathode at the stesalite frame which have a dielectric
 190 constant $\epsilon_r \approx 6$, see discussion in [14]. A strong correlation exists between the
 191 vertical position of the physical peak and the relative position of the satellites
 192 in the x -plane. Typical distances between the satellites are 82–86 cathode chan-
 193 nels reflecting the height of the frame. The satellite signals were not be present
 194 in single-track events after a fine adjustment of the integration gate, but could
 195 not be avoided in multi-track events, when the integration gate was offset in
 196 respect to the timing of the second traversing particle, and the integration be-

197 came sensitive to charges induced on the cathode strips by charges flowing out
198 of the anode wires.

199 Each cluster is further analysis for its internal structure to identify possible
200 peak positions as follows: A truncated cluster is created around the channel
201 with the charge maximum, x_{max} . It extends to the left and to the right for 2
202 channels, if the charge values for these channels are below a minimum of 90 %
203 of the charge in x_{max} . The truncated cluster extends at most up to the limits
204 of the original cluster or up to a channel with only a minimum of charge. For
205 clusters that reach the 8-bit maximum of the ADC the counting of channels
206 starts at the left and right limits of the saturation plateau. If no such structure
207 is found the cluster is discarded. This procedure ensured that a truncated
208 cluster corresponds to a peak-like structure. Next, the summed charge in the
209 truncated cluster is compared to the charge outside the peak region. If the
210 latter is larger than 30 % in the x -planes of the MWPC or larger than 1 % in
211 the y -planes of the MWPC and the outside region is wider than the required
212 minimum for a cluster, a separate cluster is created. The difference between
213 the x - and y -planes is attributed to the different appearances of pick-up charges
214 on the cathode wires. The extensions of the new cluster is depending on the
215 distribution of charges. For a large charge close to the original peak, *i.e.* within
216 2 channels, the new cluster extends to the peak region, otherwise to the border
217 region. This construction avoids the creation of extra clusters when fluctuations
218 appear in the tails of the original peak.

219 **4. Track Reconstruction**

220 In the analysis of the data all clusters are combined to form possible particle
221 tracks. With n clusters n^2 possible track points and n^4 possible tracks through
222 both chambers are generated. This ensemble is classified according to a set of
223 track quality factors, ranging from 0 (excluded) to 1 (highest quality).

224 As the MWPCs were constructed with symmetric cathode planes, a corre-
225 lation exists between the induced charge measured in one cathode plane to the

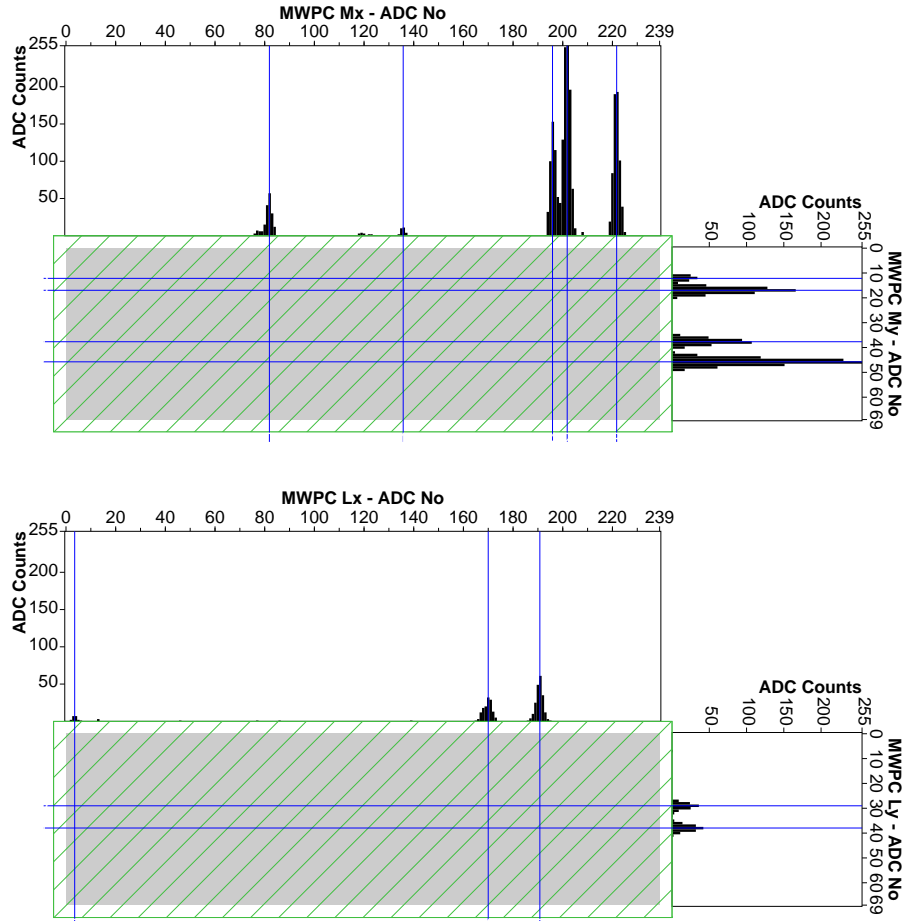


Figure 2: Charge distribution in both MWPCs of an event taken with $2\ \mu\text{A}$ beam current, corresponding to luminosities of $2.5 \times 10^{36}\ \text{cm}^2\text{s}^{-1}$. The anode wires are shown schematically as diagonal lines, cathode wires run horizontally and vertically. The grey shaded area corresponds to the active region of a chamber. Peak positions are determined by calculating the centre-of-charge from a restricted number of cathode channels and are indicated by vertical and horizontal lines in the display. The peak-finding algorithm assumes a typical peak FWHM of 3–5 cathode strips and allows for asymmetric tails inherent to the chamber geometry.

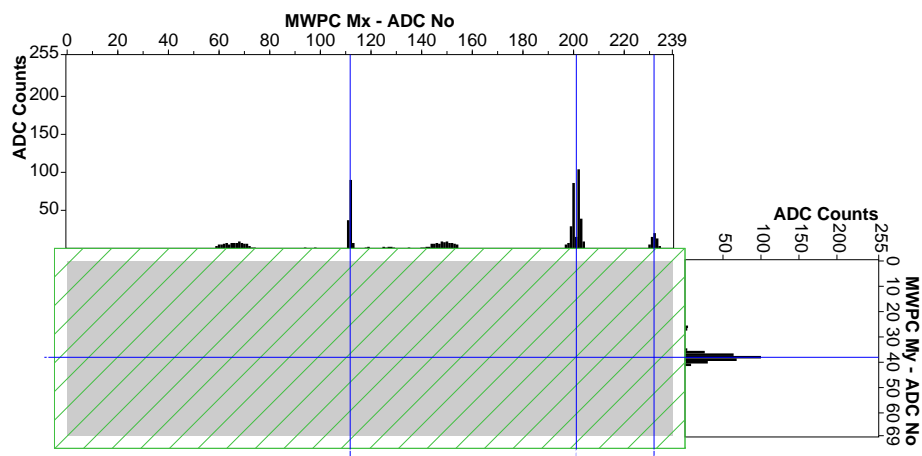


Figure 3: Charge distribution in MWPC M showing satellite charges on both sides of a needle-like peak in the x -plane. Such distributions are formed by multiple particles traversing the chamber at different times, so that the integration time window is offset and the integration is sensitive to charges induced on the cathode strips by charges flowing out of the anode wires. The coupling is seen by comparing the end-points of the diagonal anode wire crossing the vertical line of the needle peak to the position of the satellite peaks. The peak-finding algorithm rejects those satellites on the basis of their shape.

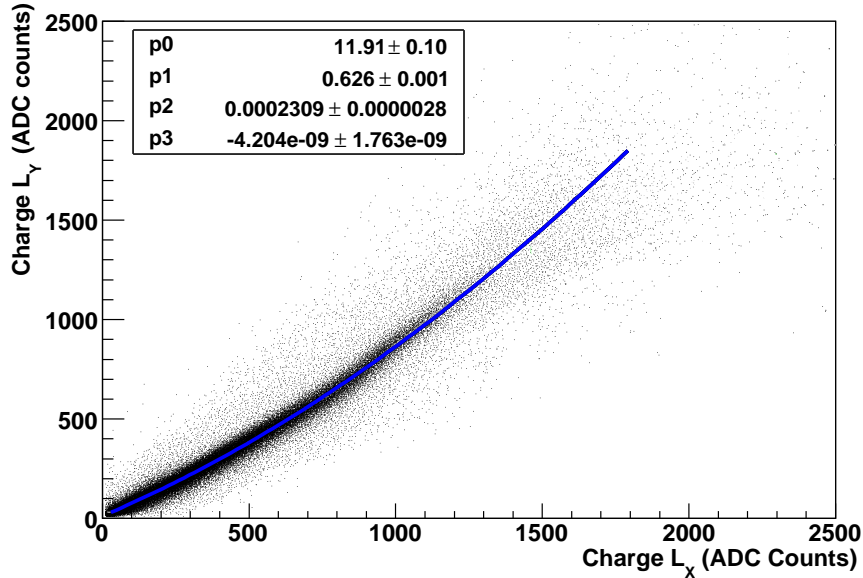


Figure 4: Correlation of induced charges on the cathode planes x and y in MWPC L. A third order polynomial function is used to parametrise phenomenologically the distribution.

226 induced charge of the perpendicular plane. Fig. 4 shows a large set of measured
 227 charges in MWPC L deposited by particles of different velocities. A third order
 228 polynomial function was used to parametrise phenomenologically the distribu-
 229 tion. The non-linear response is attributed to many factors, the asymmetry in
 230 the liberated charges drifting through the two-step MWPC, the systematics in
 231 the cluster-finding, and saturation in the ADCs. In each MWPC the measured
 232 difference of a pair of clusters in x - and y -direction to the phenomenological
 233 curve is used to determine the quality factors $Q_x/Q_y|_L$ and $Q_x/Q_y|_M$. In many
 234 cases with these factors alone a correct pairing of clusters is possible, as shown
 235 in Fig. 2.

236 Valid tracks are bound to angular limits, given by the acceptance of the
 237 spectrometer. Both MWPCs are situated in a field-free space, so that particle
 238 tracks can be extrapolated linearly to the field boundary at the end of the dipole.

239 Especially the relation between vertical hit positions of the two chambers

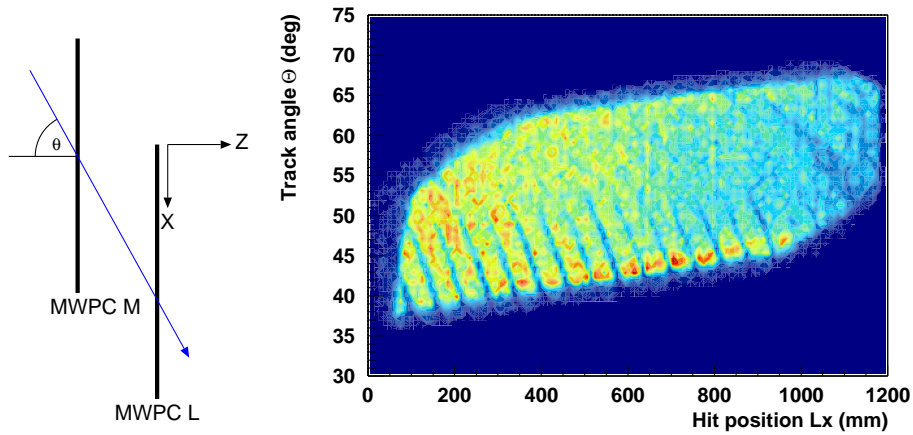


Figure 5: Left: Top view of the MWPCs in the KAOS spectrometer with the definition of the coordinate system and the horizontal track angle. Right: Distribution of events in the $x - \theta$ plane. The MWPC acceptance is formed by the bright region. The strip structures within the acceptance region are due to the geometry of the scintillator walls that leads to inefficiencies.

240 provides a powerful criterion for the track finding. The target angle acceptance
 241 of the spectrometer is large in the horizontal direction and small in the vertical
 242 direction. The vertical track angles, ϕ , for particles originating at the target are
 243 strongly correlated to the vertical positions. This $y - \phi$ relation is caused by
 244 the magnet optics leading to diverging particles tracks.

245 In the horizontal direction the tracks originating at the target form a large,
 246 but limited acceptance region with horizontal track angles, θ , ranging from 35
 247 to $\approx 70^\circ$, with a dependence on the horizontal position as shown in Fig. 5. The
 248 strip structures within the acceptance region $x - \theta$ are due to the geometry of
 249 the scintillator walls that leads to inefficiencies.

250 In the KAOS spectrometer the MWPCs are followed by two scintillator walls,
 251 labelled F and G, that are segmented in x -direction. A last group of quality
 252 factors is determined by the extrapolation of the track to both scintillator walls.
 253 The spatial difference to the closest observed hit, $\Delta x|_F$ and $\Delta x|_G$, are used as
 254 well as the the spacial difference to the vertical positions, $\Delta t|_F$ and $\Delta t|_G$, as
 255 measured by the top–bottom time differences by the individual scintillator pad-

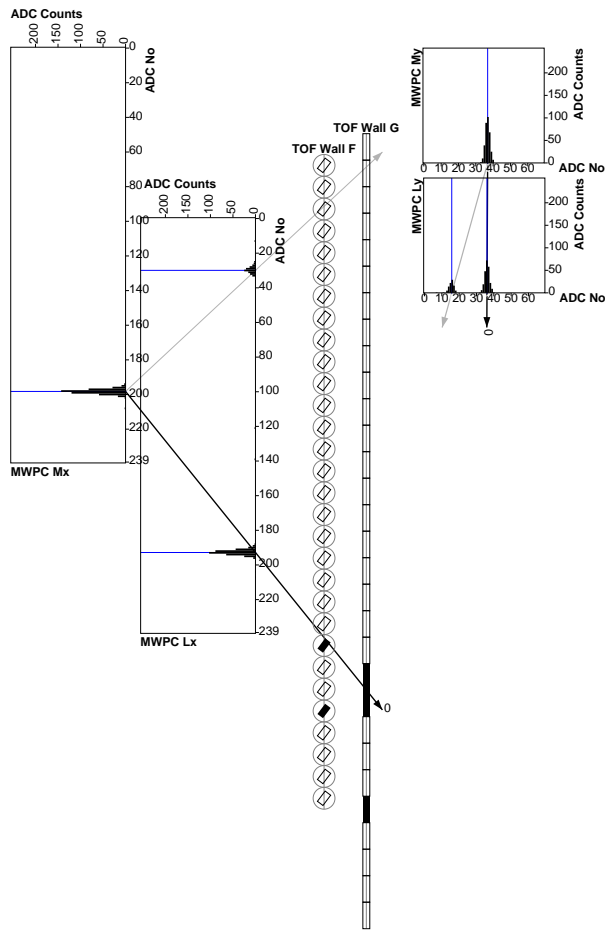


Figure 6: Display of an exceptionally simple event showing in black the ADC charges read from the x -planes of the MWPCs (left), the hits in the scintillator walls F and G (centre) and the ADC charges read from the y -planes (top right). Particles are originating in the top-left corner. One unique set of clusters in the MWPCs together with hits in the walls form the track (black arrow), the two other track combinations were excluded by the quality criteria. The track quality was close to 1, see Table 1.

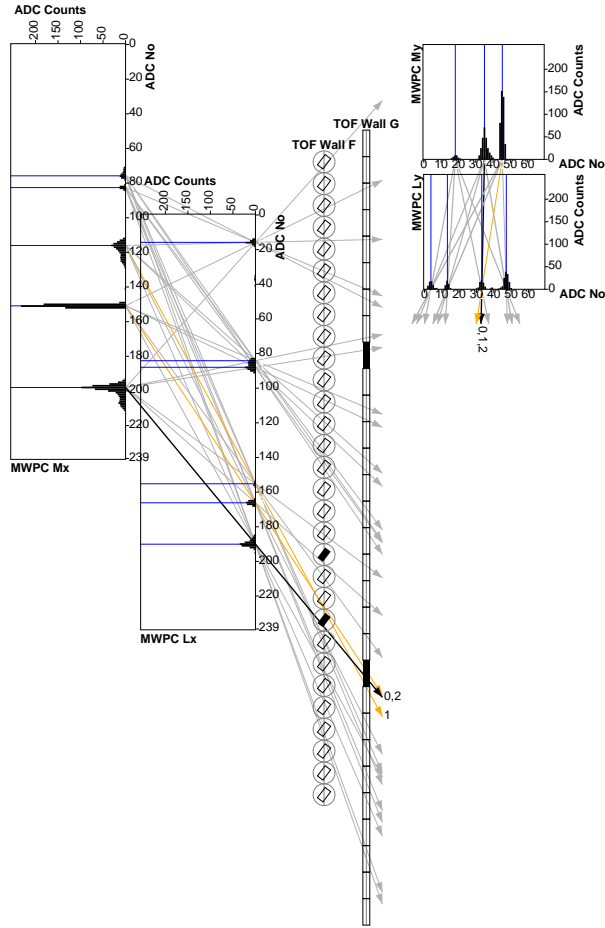


Figure 7: Same as Fig. 6 but for a more common event topology with multiple clusters or hits in each detection plane. From the charge distribution in the x -plane of MWPC M the coincident passing of one heavily ionizing and at least one minimum ionizing particle through this chamber can be deduced. The track-finding algorithm returned three possible tracks (accentuated arrows, listed in Table 1), all other cluster and hit combinations were excluded by at least one of the quality criteria.

Table 1: Track qualities for the two events displayed in Figs. 6 and 7. The quality factors Q_x/Q_y relate the charges in the two orthogonal cathode planes, the quality factors for the positions *vs.* cartesian angles $x - \theta$ and $y - \phi$ correspond to the spectrometer acceptance, the quality factors Δx correspond to the spatial difference of the projection of the track to the hit positions in the scintillator walls F and G , and the quality factors Δt correspond to the spacial difference of the projection of the track to the vertical positions as measured by the top–bottom time difference by the scintillator paddles of the walls. It is known that track no. 0 is the proper track, as explained in Section 5.

event	track	total	$Q_x/Q_y _M$	$Q_x/Q_y _L$	$x - \theta$	$y - \phi$	$\Delta x _F$	$\Delta x _G$	$\Delta t _F$	$\Delta t _G$
Fig. 6	0	0.96	1	1	1	1	1	0.96	0.58	1
Fig. 7	0	1	1	1	1	1	1	1	0.81	1
	1	0.73	0.86	0.86	1	1	1	1	0.81	1
	2	0.40	0.55	1	1	1	0.73	1	0.91	1

256 dles. The measured time difference in a scintillator bars becomes less accurate
257 when the particle deposits only a small amount of energy, *e.g.* for grazing inci-
258 dence. To improve the quality assessment the maximum value from both walls
259 is used as quality factor.

260 Figs. 6 and 7 show the event displays of two events, the first being exception-
261 ally simple with a low occupancy of ADC charges and hits in the scintillator
262 walls. It can be seen in this event that a strong charge correlation between
263 the two peaks in x - and the two peaks in y -direction exists. One unique set of
264 clusters in the MWPCs together with hits in the walls form the track, the two
265 other track combinations were excluded by the quality criteria and assigned to
266 background particles. The track quality was close to 1, see Table 1. A more
267 common event topology with multiple clusters or hits in each detection plane is
268 shown in Fig. 7. From the charge distribution in the x -plane of MWPC M the
269 coincident passing of one heavily ionizing and at least one minimum ionizing
270 particle through this chamber can be deduced. The track-finding algorithm re-
271 turns three possible tracks see Table 1), all other cluster and hit combinations
272 were excluded by one of the quality criteria. As both events were triggered by

273 the efficiency counters, explained in Section 5, it is known that with track no. 0
274 a proper track assignment was achieved.

275 **5. Tracking Efficiencies**

276 The implemented read-out principle allows for high track multiplicities, how-
277 ever, the track reconstruction can then become a major source of detection inef-
278 ficiency, quantified by the tracking efficiencies as follows: (i) intrinsic efficiency:
279 the percentage of events in which any charge was detected in the chamber fol-
280 lowing a charged particle, (ii) any track efficiency: the percentage of events in
281 which a track was reconstructed from the charges, (iii) track reconstruction ef-
282 ficiency: the percentage of events in which the proper track was reconstructed.
283 All efficiencies are to some extent depending on the cluster analysis and the
284 reconstruction method. The track reconstruction efficiency is heavily depend-
285 ing on the particle's momentum and the beam current, or more general on the
286 luminosity. The latter dependency is a consequence of the fast increment of the
287 flux of background particles with the current.

288 There is no way of determining the tracking efficiencies from the electro-
289 production measurements. Instead, data was taken during dedicated efficiency
290 runs. For these runs two small scintillating detectors of type Bicron BC-408 and
291 dimensions $L \times W \sim 30 \times 20 \text{ mm}^2$ with 5 mm thickness were installed in front
292 of each MWPC to determine intrinsic and tracking efficiencies of the chambers.
293 The active parts were connected to optical light guides and read out by PMTs of
294 type Hamamatsu R1828. When attached to the MWPC frames the active areas
295 of the counters were vertically centred and horizontally at the same position
296 relative to the corresponding MWPC. The detectors could easily be moved out
297 of the spectrometer's acceptance when not in use.

298 The external counters could be used to select trajectories passing through
299 both chambers in a small acceptance region. The histogram in Fig. 8 shows a
300 typical distribution of events in the wire chamber coordinate system obtained
301 under those trigger conditions for a beam current of $4 \mu\text{A}$, corresponding to

302 luminosities of $5 \times 10^{36} \text{ cm}^2\text{s}^{-1}$. The bands in x - and y -direction correspond
 303 to wrongly reconstructed coordinates in one of the four MWPC planes, the
 304 strongly populated square corresponds to the projection of the position of the
 305 efficiency counters. When requiring a high track quality almost only properly
 306 reconstructed tracks remain in the event sample.

307 The spectrometer was situated under forward angles at 31° with a solid an-
 308 gle acceptance of $\Omega \approx 10 \text{ msr}$ in an in-plane angular range of $\vartheta = 21 - 43^\circ$. The
 309 results are separated into samples taken with 1, 2, 3, and $4 \mu\text{A}$ beam current and
 310 within the samples into events where the traversing particle was identified by its
 311 specific energy-loss as proton and pion by the scintillator walls. With the spec-
 312 trometer set to a momentum bite around $600 \text{ MeV}/c$ protons, kaons, and pions
 313 loose significantly different energies in the counter gas. The intrinsic efficiencies
 314 were well above 99% independent on the beam current. The efficiency to form
 315 a track was somewhat above 98%. For pions track reconstruction efficiencies
 316 ranged between 86 and 68% corresponding to beam currents of $1-4 \mu\text{A}$, for pro-
 317 tons the efficiencies were between 98 and 90%, details are tabulated in Table 2.
 318 Several runs were taken during a period of 2 weeks showing small variations of
 319 no more than 2%. Charge-separated tracking efficiencies for a beam current of
 320 $4 \mu\text{A}$ are shown in Fig. 9. From the average charge collected for kaons track
 321 reconstruction efficiencies of 75–90% were evaluated.

322 Tracks reconstructed to pass through the acceptance region on average have
 323 a higher quality factor, whereas tracks reconstructed to miss this region on
 324 average have a smaller quality factor. The continuous increase of the efficiency
 325 with the quality as shown in Fig. 10 for $4 \mu\text{A}$ beam current, provides confidence
 326 that the quality factor is indeed a measure of the goodness-of-track.

327 6. Discussion

328 When using the cathode-charge sampling method for the bi-dimensional
 329 read-out of MPWCs a large variation of induced charge distributions can be
 330 observed, depending *e.g.* on track angles, charged particle velocities, integration

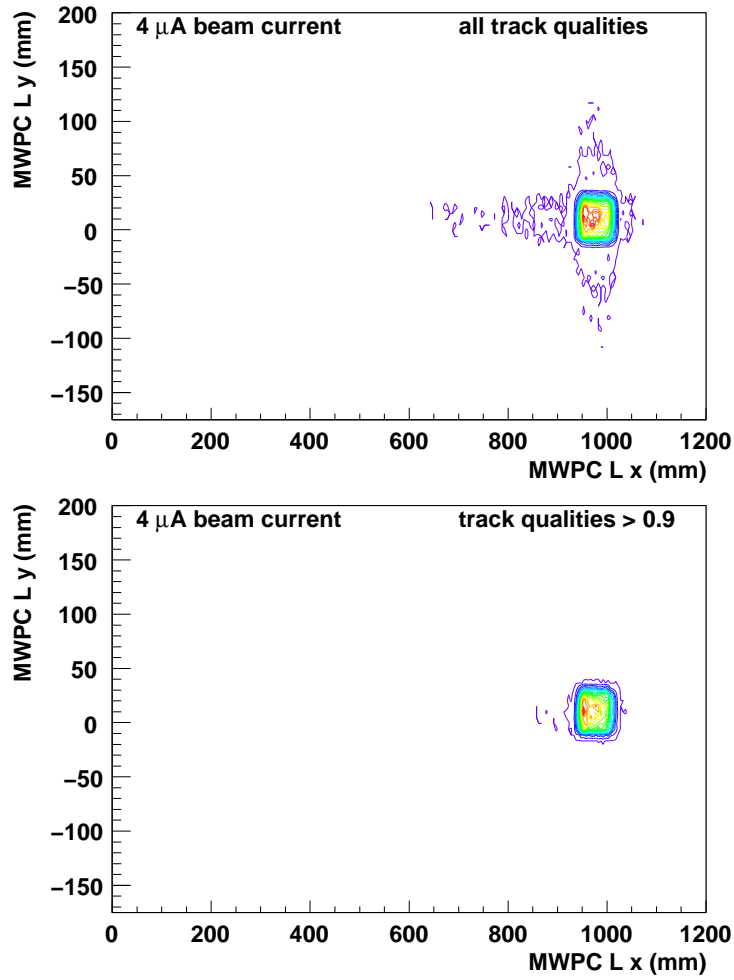


Figure 8: Reconstructed track positions in MWPC L for events triggered by the efficiency counters at a beam current of $4\ \mu\text{A}$ for all track qualities (top) and for track qualities larger 0.9 (bottom). The densely populated square (approx. $93 \times 58\ \text{mm}^2$) corresponds to the projection of the position of the efficiency counters to the wire chamber coordinate system which defines the acceptance region of this chamber. Tracks found to be outside of this acceptance region were reconstructed wrongly. These tracks tend to have a low track quality.

Table 2: Intrinsic particle detection and tracking efficiencies as determined with the efficiency counter set-up. A track is defined as being properly reconstructed if it is found to be in the acceptance region of the respective chamber. The gain was higher in chamber L than in chamber M, so that tracking efficiencies differ by a few percent, this difference is increasing with beam current. The chamber track reconstruction efficiencies in columns 5 and 6 include all track qualities from 0 to 1 and all particle species. These efficiencies are separated into pion and proton tracks. Larger inefficiencies arise for higher beam currents and for pion tracks due to the resulting ambiguities and distortions in the charge distributions. The bottom 3 lines show the loss of efficiency when not all quality factors are used in the track reconstruction.

$\mathcal{L}/10^{36}$ (cm^2s^{-1})	I (μA)	intrinsic ϵ (%)		tracking ϵ (%)			proton ϵ (%)		pion ϵ (%)		used quality factors
		L	M	any track	L	M	L	M	L	M	
1.2	1	99.3	99.6	97.8	97.1	95.9	98.3	97.1	86.4	83.9	all
2.5	2	99.5	99.7	97.6	96.0	93.4	97.4	95.1	83.5	78.4	"
3.7	3	99.6	99.8	97.3	94.5	90.9	96.0	92.7	81.7	74.9	"
5	4	99.6	99.8	97.3	93.1	88.2	95.0	90.6	76.9	67.9	"
5	4	"	"	98.9	75.8	62.7	78.2	65.5	54.3	39.0	no $\Delta x _{F,G}$, no Δz
5	4	"	"	97.8	90.6	80.8	92.5	83.8	74.0	55.8	no $x - \theta$, no $y - \theta$
5	4	"	"	97.9	91.4	83.7	93.1	85.8	77.1	66.5	no $Q_x/Q_y _{M,L}$

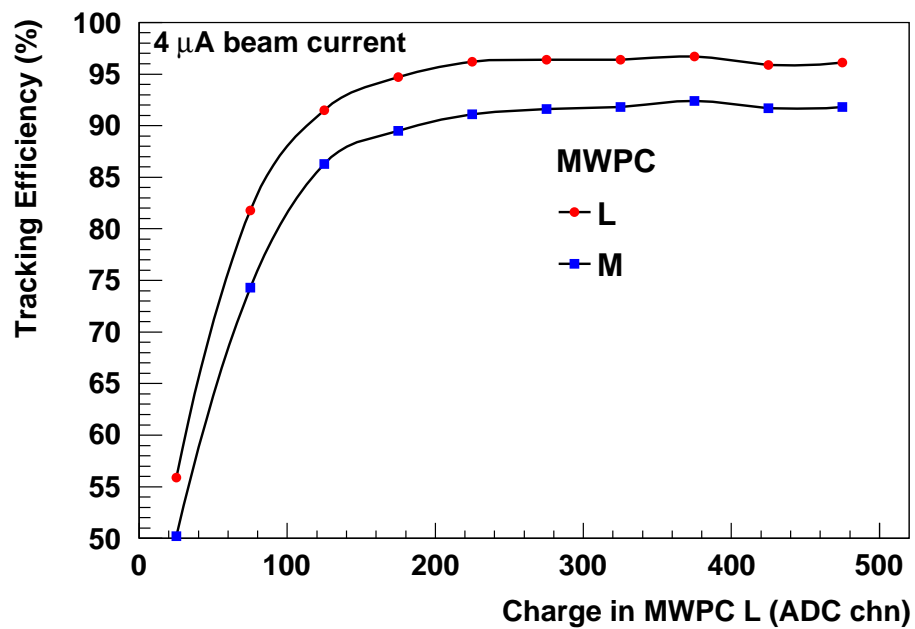


Figure 9: Charge-separated track reconstruction efficiencies for a beam current of $4\ \mu\text{A}$. Efficiencies for both chambers are shown as a function of induced charge on the cathode of MWPC L. The average charge collected in chamber L for pions is ~ 65 ADC counts, and for protons ~ 220 ADC counts.

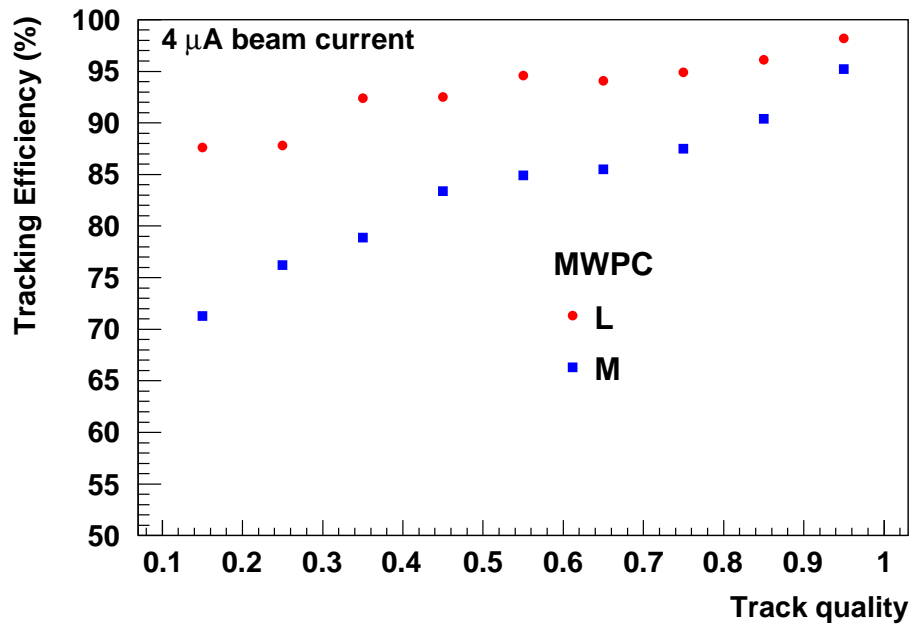


Figure 10: Quality-separated track reconstruction efficiencies for a beam current of $4 \mu\text{A}$. Efficiencies for both chambers are shown as a function of a quality factor that includes, among others, the correlation that exists between the induced charge measured in one cathode plane to the induced charge of the perpendicular plane and the relation between vertical hit positions in the two chambers. The continuous increase of the efficiency with the quality provides confidence that the quality factor is indeed a measure of the goodness-of-track.

331 gate width and timing, and charged particle occupancies. For MWPCs used
332 as tracking detectors in a magnetic spectrometer these factors vary, as incident
333 particle species and momenta as well as background particle fluxes depend on
334 the spectrometer and accelerator settings for a particular experiment.

335 To resolve the ambiguities appearing with multiple, non-perpendicular inci-
336 dent particles with different energy-losses a cluster-finding and track reconstruc-
337 tion algorithm was developed that assigns each possible track a quality factor.
338 This method was in-beam tested with two large-sized MWPCs in the KAOS
339 spectrometer and proved to be effective not only in quantifying the tracking
340 efficiencies, but more importantly it allowed to systematically determine track
341 reconstruction efficiencies which can be applied to the operation of the MWPCs
342 in electro-production experiments.

343 In general, tracks of heavily ionising particles in a low background environ-
344 ment have the largest probability of being properly reconstructed. Tracks of
345 minimum ionizing particles are harder to reconstruct properly as background
346 signals of dominantly small amplitudes are present in the chambers at any time.
347 It is concluded that the track reconstruction in the MWPCs represents a pri-
348 mary source of inefficiency for high electron beam currents on typical targets of
349 several hundred mg/cm^2 thickness. The use of information from the external
350 detectors improves the efficiencies by 20–25 % in the case of the highest beam
351 current that was probed. However, at these currents also the external counters
352 register many multiply hits. The check on the spectrometer acceptance and
353 the correlations of the coordinates improves the efficiencies by 10–15 %, and
354 the induced cathode charge correlation has an impact of $\sim 5\%$ for the higher
355 amplitudes.

356 By using the introduced method and the obtained results the track recon-
357 struction efficiencies for particles not seen in the beam-tests, *i.e.* kaons, could
358 have been determined. These findings were applied to data taken with the KAOS
359 spectrometer in kaon electro-production, improving the systematic uncertainties
360 in the cross-section extraction significantly.

361 **Acknowledgements**

362 Work supported in part by the Federal State of Rhineland-Palatinate and by
363 the Deutsche Forschungsgemeinschaft with the Collaborative Research Center
364 443.

365 **References**

- 366 [1] K. I. Blomqvist, High resolution magnetic spectrometers, Nucl. Phys. A
367 497 (1989) 457c–464c.
- 368 [2] O. K. Baker, et al., The High Momentum Spectrometer drift chambers in
369 Hall C at CEBAF, Nucl. Instr. and Meth. in Phys. Res. A 367 (1995) 92–95.
- 370 [3] K. I. Blomqvist, et al., The three-spectrometer facility at the Mainz mi-
371 crotron MAMI, Nucl. Instr. and Meth. in Phys. Res. A 403 (3) (1998)
372 263–301.
- 373 [4] K. G. Fissum, et al., Vertical drift chambers for the Hall A high-resolution
374 spectrometers at Jefferson Lab, Nucl. Instr. and Meth. in Phys. Res. A 474
375 (2001) 108–131.
- 376 [5] T. Miyoshi, et al., High resolution spectroscopy of the ${}_{\Lambda}^{12}\text{B}$ hypernucleus
377 produced by the $(e, e'K^+)$ reaction, Phys. Rev. Lett. 90 (23) (2000) 232502.
- 378 [6] T. Gogami, Medium heavy hypernuclear spectroscopic experiment JLab
379 E05-115, in: 22nd Indian-Summer School on Strangeness Nuclear Physics
380 (SNP2010), Rez/Prague, Czech, 7–11 September 2010.
- 381 [7] Induced charge distributions in proportional detectors, Brookhaven
382 National Laboratory Instrumentation Publication, online available at
383 <http://www.inst.bnl.gov/publications/Mathieson.shtml> (1991).
- 384 [8] P. Achenbach, et al., First measurements of Λ and Σ^0 hyperons in elemen-
385 tary electroproduction at MAMI, in: B. F. Gibson, K. Imai, T. Motoba,

- 386 T. Nagae, A. Ohnishi (Eds.), Proceedings of the X International Confer-
387 ence on Hypernuclear and Strange Particle Physics (HypX), Tokai, Japan,
388 14–18 September 2009, Nucl. Phys. A 835 (2010) 313–316.
- 389 [9] H. Stelzer, Multiwire chambers with a two-stage gas amplification, Nucl.
390 Instr. and Meth. in Phys. Res. A 310 (1991) 103–106.
- 391 [10] P. Senger, et al., The kaon spectrometer at SIS, Nucl. Instr. and Meth. in
392 Phys. Res. A 327 (2–3) (1993) 393–411.
- 393 [11] A. Breskin, G. Charpak, S. Majewski, G. Melchart, G. Petersen, F. Sauli,
394 The multistep avalanche chamber: a new family of fast, high-rate particle
395 detectors, Nucl. Instr. and Meth. 161 (1979) 19–34.
- 396 [12] G. Charpak, F. Sauli, High-accuracy, two-dimensional read-out in multiwire
397 proportional chambers, Nucl. Instr. and Meth. 113 (1973) 381–385.
- 398 [13] N. Awaji, et al., Resolution study of cathode-charge sampling on a multi-
399 wire proportional chamber for accurate particle tracking, Nucl. Instr. and
400 Meth. 198 (1982) 243–251.
- 401 [14] P. Baltes, C. Müntz, H. Oeschler, S. Sartorius, A. Wagner, H. Stelzer,
402 Properties of large MWPC’s at the Kaon Spectrometer, in: GSI Scientific
403 Report 1991, GSI, Darmstadt, 1992, p. 364.